Received: 22 September 2021 | Accepted: 26 October 2021

DOI: 10.1002/iub.2576

SPECIAL ISSUE

IUBMB LIFE WILEY

Cofactors and pathogens: Flavin mononucleotide and flavin adenine dinucleotide (FAD) biosynthesis by the FAD synthase from *Brucella ovis*

Andrea Moreno[1,2,3] | **Victor Taleb**[1,2] | **María Sebastián**[1,2] | **Ernesto Anoz-Carbonell**[1,2] | **Marta Martínez-Júlvez**[1,2] | **Milagros Medina**[1,2]

[1]Departamento de Bioquímica y Biología Molecular y Celular, Facultad de Ciencias, Universidad de Zaragoza, Zaragoza, Spain

[2]Instituto de Biocomputación y Física de Sistemas Complejos, BIFI (GBsC-CSIC Joint Unit), Universidad de Zaragoza, Zaragoza, Spain

[3]Departamento de Biología, Facultad de Ciencias, Universidad de Los Andes, Mérida, Venezuela

Correspondence
Marta Martínez-Júlvez and Milagros Medina, Departamento de Bioquímica y Biología Molecular y Celular, Facultad de Ciencias, Pedro Cerbuna 12, Universidad de Zaragoza, 50009 Zaragoza, Spain.
Email: mmartine@unizar.es (M. M.-J.) and mmedina@unizar.es (M. M.)

Funding information
Government of Aragón-FEDER, Grant/Award Number: E35_20R; Spanish Ministry of Science and Innovation-State Research Agency, Grant/Award Number: PID2019-103901GB-I00

Abstract

The biosynthesis of the flavin mononucleotide (FMN) and flavin adenine dinucleotide (FAD), cofactors used by 2% of proteins, occurs through the sequential action of two ubiquitous activities: a riboflavinkinase (RFK) that phosphorylates the riboflavin (RF) precursor to FMN, and a FMN:adenylyltransferase (FMNAT) that transforms FMN into FAD. In most mammals two different monofunctional enzymes have each of these activities, but in prokaryotes a single bifunctional enzyme, FAD synthase (FADS), holds them. Differential structural and functional traits for RFK and FMNAT catalysis between bacteria and mammals, as well as within the few bacterial FADSs so far characterized, has envisaged the potentiality of FADSs from pathogens as targets for the development of species-specific inhibitors. Here, we particularly characterize the FADS from the ovine pathogen *Brucella ovis* (BoFADS), causative agent of brucellosis. We show that BoFADS has RFK activity independently of the media redox status, but its FMNAT activity (in both forward and reverse senses) only occurs under strong reducing conditions. Moreover, kinetics for flavin and adenine nucleotides binding to the RFK site show that BoFADS binds preferentially the substrates of the RFK reaction over the products and that the adenine nucleotide must bind prior to flavin entrapment. These results, together with multiple

Abbreviations: ANP, adenine nucleotide (ATP or ADP); Bo, *Brucella ovis*; Bs, *Bacillus subtilis*; Ca, *Corynebacterium ammoniagenes*; CD, circular dichroism; Ec, *Escherichia coli*; ESKAPE, acronym comprising the scientific names of six highly virulent and antibiotic resistant bacterial pathogens; FADS, FAD synthase; FLV, flavin nucleotide (RF, FMN or FAD); FMNAT, ATP:FMN adenylyltransferase; HPLC, high-performance liquid chromatography; Hs, *Homo sapiens*; k_{cat}, catalytic constant; K_d, dissociation constant; K_i, inhibition constant; K_M, Michaelis constant; k_{obs}, observed rate constant; k_{off}, dissociation rate constant; k_{on}, association rate constant; Lm, *Listeria monocytogenes*; Mt, *Mycobacterium tuberculosis*; PIPES, 1,4-piperazine diethane sulphonic acid; PPi, pyrophosphate; RF, riboflavin, vitamin B2; RFK, ATP:riboflavin kinase; Sa, *Staphylococcus aureus*; SDS–PAGE, sodium dodecyl sulfate–polyacrylamide gel electrophoresis; Spn, *Streptococcus pneumoniae*; ε, extinction coefficient.

sequence alignments and phylogenetic analysis, point to variability in the less conserved regions as contributing to the species-specific features in prokaryotic FADSs, including those from pathogens, that allow them to adopt alternative strategies in FMN and FAD biosynthesis and overall flavin homeostasis.

KEYWORDS

enzyme kinetics, enzyme species-specific traits, flavin biosynthesis, FMN: adenylyltransferase, kinetics limiting steps, riboflavin kinase

1 | INTRODUCTION

In organisms from all kingdoms, the riboflavin kinase activity (RFK; EC 2.7.1.26) is mandatory for the biosynthesis of the flavin mononucleotide (FMN) cofactor, using as substrates riboflavin (RF, vitamin B2) and ATP.[1–7] FMN is also the precursor of the flavin adenine dinucleotide (FAD) cofactor, the most abundant flavin cofactor in flavoproteins, that is synthesized through a FMN:adenylyltransferase activity (FMNAT; EC 2.7.7.2).[8] As cofactors of flavoproteins FMN and FAD are key metabolites for the maintenance of life and are involved in a wide range of physiological processes.[7,9–11] These include biomolecular networks that regulate different cellular processes, such as cellular development, activation of defense reactive oxygen species and signaling molecules; or the expression of other proteins (as flavin transporters) through FMN riboswitches.[12–16] Proteins holding RFK activity have similarity in sequence, overall folding and structural arrangement in all species. Thus, the prokaryotic RFK protein is a domain fused to another domain that is involved in the biosynthesis of FAD, using FMN and ATP as substrates, and therefore has FMNAT activity (Figure 1).[17,18] For this reason, the prokaryotic bifunctional enzyme is usually referred to as FAD synthase (FADS). In many FADSs, the FMNAT activity is reversible, so that these enzymes also have FAD pyrophosphorylase (FADpp) activity. Noticeably, the

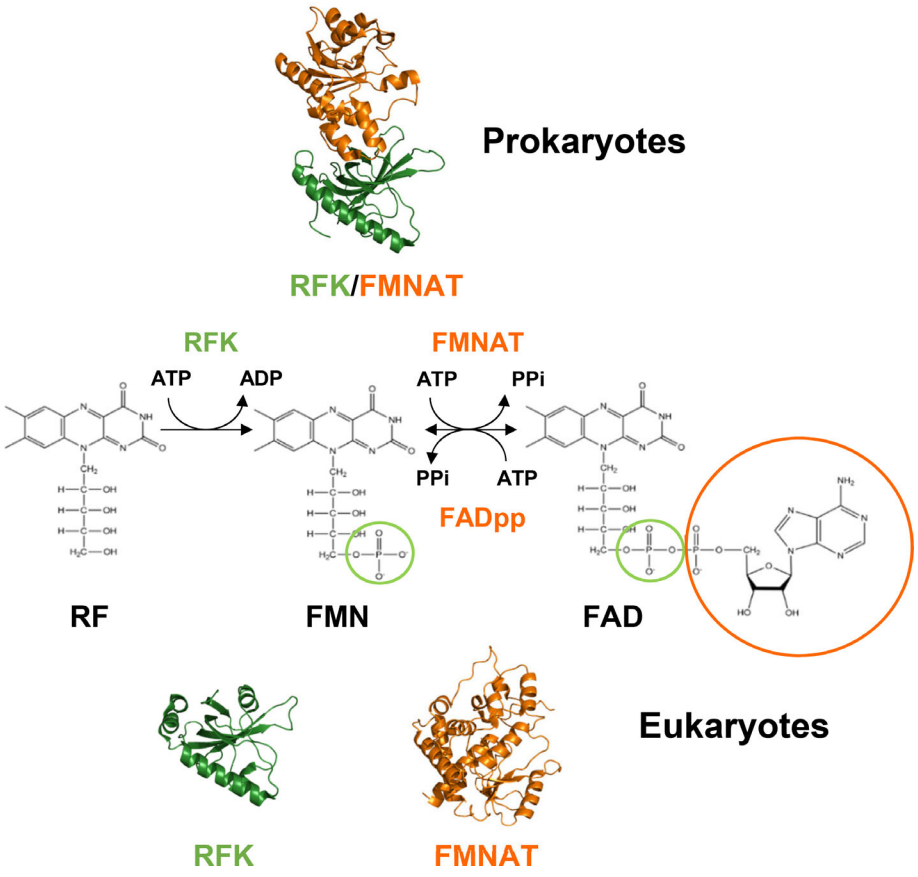

FIGURE 1 Scheme of the reactions catalyzed by prokaryotic bifunctional FADSs and the corresponding eukaryotic monofunctional enzymes. 3D structures of prokaryotic CaFADS (PDB 2X0K), monofunctional HsRFK (PDB 1NB0) and monofunctional FMNAT from *Candida glabrata* (PDB 3FWK) are drawn in cartoon and colored by the catalyzed activity (orange for FMNAT and green for RFK)

prokaryotic FMNAT domain is not homologue to monofunctional mammalian FADSs in sequence, structure or chemistry for catalysis.[3,4,18,19]

Although homology is clear among domains and proteins catalyzing RFK activity, species-specific features in RFK ligand binding and catalysis are reported among the few FADSs thoroughly evaluated in bacteria, which include *Corynebacterium ammoniagenes* (CaFADS), *Listeria monocytogenes* (LmFADS), *Staphylococcus aureus* (SaFADS), *Bacillus subtilis* (BsFADS) and *Streptococcus pneumonia* (SpnFADS). There are enzymes with RFK activity inhibited by the RF substrate, or requiring reducing or oxidized conditions for functionality. Conformational arrangements during catalysis also appear particular for each protein.[3,5,17,18,20–22] These observations exemplify different strategies to control flavin homeostasis through regulation of FMN biosynthesis. As bacterial FADSs are required to provide flavins to 2% of the total proteome of the organisms, both of their activities might result interesting targets for the discovery of specific antimicrobials.[8,23,24] In this context, the understanding of RFK and FMNAT activities traits in different species, as well as of the mechanisms for FMN and FAD delivery to the client apo-proteins, are essential aspects to investigate.

Here, we report on the characterization of the FADS from *Brucella ovis* (BoFADS), a pathogen provoking placentitis in sheep and genital lesions in rams, which affect the semen quality and the fertility, incrementing the animal management cost.[25–27] During the infective processes, bacteria penetrate the host mucosa and enter into phagocytic macrophages, where they replicate and escape host immunity, being this process essential for virulence and the establishment of chronic infections.[28] Several flavin-dependent proteins are envisaged to participate in these processes, making the FMN and FAD supply critical for bacterial infection.[29–32] Our steady-state characterization of the heterologously overexpressed BoFADS indicates that its RFK activity does not exhibit inhibition by substrates and takes place under both reducing and oxidizing conditions with similar efficiency, whereas FMNAT and FADpp activities require strong reducing conditions to occur. Moreover, stopped-flow spectrophotometry allows ascertaining sequential conformational changes upon ligand binding and catalysis at the RFK site. When evaluated in the context of the knowledge of other RFK and FMNAT activities as well as sequence conservation and evolution within family members, these results exemplify how subtle changes in protein sequence or conformation allow different organisms to adopt alternative strategies in FMN and FAD biosynthesis and homeostasis.

2 | EXPERIMENTAL PROCEDURES

2.1 | Cloning, expression and purification of proteins

The *ribF* gene (BOV_A0180/BOV_RS11255/) coding for BoFADS (ABQ62831.1) was synthesized by *GenScript*, applying codon optimization for its heterologous expression in *Escherichia coli*, and cloned between the *Nco*I and *Bam*HI restriction sites of a pET28a(+) vector, including a His_6-tag tail and the PreScission Protease cleavage signal at the 5′ end. The resulting pET28a-BoFADS plasmid was transformed into *E. coli* BL21(DE3) strain cells, which were grown at 37 °C in Luria Bertani medium (1% [wt/vol] tryptone, 0.5% [wt/vol] yeast extract and 1% [wt/vol] NaCl) supplemented with 50 mg/mL of kanamycin. At an OD_{600nm} of 0.8, cultures were induced with 0.5 mM isopropyl β-D-1-thiogalactopyranoside, incubated under the same conditions for 24 h and then harvested. Cells were resuspended in 20 mM potassium phosphate, pH 7.4, 10 mM imidazole and 0.5 M NaCl, and containing the protease inhibitor phenylmethylsulphonyl fluoride (1 μM). Purification of BoFADS to homogeneity was carried out following basically the procedure reported for the FADS from *S. pneumoniae*.[33] Briefly, cells were broken by sonication and centrifuged. Supernatant was loaded onto a His-Trap affinity column (HisTrap HP; GE Healthcare) and the protein was eluted applying a gradient from 10 to 500 mM imidazole in 20 mM potassium phosphate, pH 7.4. Exchange buffer to 25 mM Tris/HCl, pH 7.4, 150 mM NaCl was performed by using a HiPrep Desalting Column (GE Healthcare). The His_6-Tag was removed by 24 h incubation with the PreScission protease (GE Healthcare) at 4 °C, in ratio 2:10 (wt/wt), and then both remained His_6-tagged BoFADS and the PreScission protease were removed with HisTrap HP and GSTrap 4B connected columns. The unbound free BoFADS fraction was recovered and further purified by size exclusion chromatography using a Superdex 200 10/300 GL column (GE Healthcare) previously equilibrated with 20 mM PIPES, pH 7.0, 150 mM NaCl. Protein purity was assessed by 15% SDS–PAGE. Pure protein solutions were stored in 25 mM Tris/HCl, pH 7.4, 150 mM NaCl at −80°C. When required, the buffer was exchanged to that for each particular experiment.

2.2 | Spectroscopic analysis

UV–visible spectra were recorded in a Cary Bio100 spectrophotometer (Agilent Technologies) in 20 mM PIPES, pH 7.0 at 25 °C. BoFADS was quantified using the

theoretical extinction coefficient $\varepsilon_{280nm} = 8.94\ mM^{-1}.cm^{-1}$ (assuming all Cys residues are reduced). This value and other parameters were calculated by the ProtParam tool from Expasy, https://web.expasy.org/protparam/). Fluorescence emission spectra were recorded in a CARY Eclipse (Agilent Technologies) in 20 mM PIPES, pH 7.0 at 25 °C, exciting the protein aromatic residues at 280 nm. Fluorescence excitation scans were recorded at the maximum emission wavelength (323 nm) and in the same experimental conditions. Circular dichroism (CD) spectra were recorded at 25 °C using a Chirascan spectropolarimeter (Applied Photosystem Ltd.). Samples containing 5 and 20 μM BoFADS in 20 mM PIPES, pH 7.0, were used in the far-UV (cuvette path length, 0.1 cm) and near-UV CD (1 cm), respectively.

2.3 | In vitro detection of quaternary organizations

To assess potential assembly of BoFADS in homo-quaternary organizations, samples containing 30 ng of BoFADS (42 μM, 20 μL) in 20 mM PIPES, pH 7.0, were incubated for 30 min at room temperature both in the absence and presence of the bis(sulfosuccinimidyl) suberate (BS_3, 3.5 μM) crosslinker (Thermo Scientific). The crosslinking reaction was stopped by addition of 0.5 M Tris/HCl, pH 8.0, until a final concentration of 50 mM. Samples were then resolved by 15% SDS–PAGE.

2.4 | Qualitative detection of activities

RFK, FMNAT, and FADpp activities were qualitatively assayed by resolving flavin products from reaction mixtures by thin layer chromatography (TLC). Activity was evaluated in samples containing either 0.1 mg of crude extracts of *E. coli* BL21(DE3) cells transformed with the pET28a-BoFADS plasmid (nontransformed cells were used as control) and grown under the above indicated conditions to induce BoFADS expression, or 1 μM purified BoFADS. Unless, otherwise stated, reaction mixtures (usually 200 μL) contained 50 μM of flavins (RF, FMN or FAD), and 3.5 mM ATP (or pyrophosphate (PPi)) in 50 mM Tris/HCl pH 7.6, in the presence of 10 mM $MgCl_2$. When indicated, 10 mM sodium dithionite was used as flavin-reducing agent. Reaction mixtures were incubated at 37 °C during 15 min. Reactions were then stopped by heating the samples at 100 °C for 5 min, and supernatants were applied to Silica Gel SIL-G-25 plates, with a thickness of 0.25 mm, for the separation of flavins.[34] Flavin mixtures containing 50 μM of each flavin (RF, FMN and FAD) were included as standards. Flavin spots were examined by evaluating flavin fluorescence under UV light.

2.5 | Quantitative determination of steady-state kinetic parameters

Rates for the transformation of substrates into products were assessed by quantification of the substrates and/or products of the reaction through high-performance liquid chromatography (HPLC) after incubation of BoFADS with substrates. Gradients of pH, sodium dithionite and/or $MgCl_2$ concentrations were evaluated to select the best performing conditions. To determine kinetic parameters, k_{cat} and K_M, for the RFK activity, 50 nM BoFADS was mixed with variable concentrations of RF (0.2–15 μM) while keeping ATP constant at saturating concentration (500 μM), as well as with variable ATP (10–600 μM) and keeping RF saturating (10 μM). Reaction mixtures contained 500 μL in 20 mM Tris/HCl, pH 8.0 and 1 mM $MgCl_2$, and after adding the enzyme were incubated 5 min at 37 °C. Alternatively, RFK kinetic parameters were also evaluated in 20 mM HEPES, pH 7.0, 1 mM $MgCl_2$ for 1 min at 25 °C. Kinetic parameters for the FMNAT/FADpp activities were determined in samples mixing 500 nM BoFADS with variable concentrations of FMN/FAD (0.2–30 μM) while keeping ATP/PPi saturating (400 μM), or ATP/PPi (2–400 μM) while keeping FMN/FAD saturating (20 μM). Reaction mixtures contained 500 μL in 20 mM Tris/HCl, pH 8.0, 150 mM KCl, 10 mM $MgCl_2$ and 20 mM sodium dithionite, and were incubated 5 min at 37 °C after adding the enzyme. In all cases, reactions were stopped by heating at 100 °C for 5 min. Flavins were resolved by HPLC using an Alliance HPLC system (Waters) equipped with a 2707 autosampler and an HSST3 column (4.6 × 50 mm, 3.5 mm; Waters) preceded by a precolumn (4.6 × 20 mm, 3.5 mm; Waters) following previously reported protocols.[35,36] FMN and FAD standard curves (acquired under the same conditions) were used to quantify the FMN and FAD present at each assayed condition. The kinetic data obtained when varying the concentration of one of the substrates at saturating concentration of the other one were fitted to the Michaelis–Menten equation kinetic model, obtaining the corresponding k_{cat} and K_M values.

2.6 | Pre-steady-state binding kinetics

Kinetic experiments to evaluate rates for binding of flavins in the pre-steady state were registered using stopped-flow spectroscopy on an Applied Photophysics

SX18.MV spectrophotometer, using the ProData SX software (Applied Photophysics Ltd.) for fluorescence data acquisition and data analysis. Fast kinetic measurements were carried out at 25 °C in 20 mM PIPES, pH 7.0, 0.8 mM $MgCl_2$ and 0.3 mM NaCl, following previously described methodologies.[5,20] In short, 0.2 μM BoFADS was mixed with reaction samples containing increasing concentrations of either RF or FMN (herein FLV denotes either one of them in these experiments) ligands in the absence or presence of saturating concentrations of ATP or ADP (denoted herein as ANP) (250 μM). Evolution of flavin fluorescence after mixing was measured with an excitation wavelength of 445 nm, while fluorescence emission was recovered using a >530 nm cut-off filter. All the concentrations indicated for these experiments are the final ones in the stopped-flow observation cell. Five reproducible traces were acquired at each time and concentration condition assayed. Kinetic decays were then fitted to exponential functions,

$$y = \sum A_i \cdot \exp(-k_{obsi} \cdot t). \quad (1)$$

k_{obs} values showing a linear dependence on the FLV concentration were fitted to a one-step model associated to the binding (BoFADS + FLV ⇆ BoFADS:FLV) or to the reorganization equilibrium of the FLV ligand to BoFADS (BoFADS:FLV ⇆ BoFADS:FLV*), whose kinetics can be represented by the following equation:

$$\begin{aligned} k_{obs} &= k_{on} \cdot (FLV) + k_{off} \text{ or} \\ k_{obs-reg} &= k_{on-reg} \cdot (FLV) + k_{off-reg}, \end{aligned} \quad (2)$$

where k_{on} and k_{off} are the kinetic rate constants for complex formation and dissociation, whereas $k_{on\text{-}reg}$ and $k_{off\text{-}reg}$ are the rate constants for interconversion into two bound states with different conformation. Flavin photobleaching within the stopped-flow observation chamber was evaluated as previously described.[5]

2.7 | Sequence and structural analyses

Full-length deduced-protein sequences of a range of bacterial bifunctional FADSs were retrieved from UniProtKB (https://www.uniprot.org/) or NCBI databases (https://www.ncbi.nlm.nih.gov/genbank), choosing preferentially sequences manually reviewed and/or reference sequences (Table S1, Supporting Information). Theoretical parameters were calculated from FADS protein sequences by the ProtParam tool from Expasy (https://web.expasy.org/protparam/). Sequences were globally aligned with Clustal Omega (https://www.ebi.ac.uk/Tools/msa/clustalo/)[37] and the sequence Logo was built with WebLogo3 (https://weblogo.berkeley.edu/). For phylogeny analysis, multiple sequence alignments were trimmed through the trimAl (v.1.3) software using the automated trimming heuristic method (optimized for alignments to be analyzed by maximum likelihood).[38] The maximum likelihood phylogenetic tree was constructed with MEGA X (v.10.2.5) using the Jones–Taylor–Thornton (JTT) model.[39] Initial trees for the heuristic search were obtained automatically by applying neighbor joining and BioNJ algorithms to a matrix of pairwise distances estimated using the JTT model, and then selecting the topology with the superior log likelihood value. Bootstrap analyses with a value of 700 were performed. The final tree was visualized and edited using FigTree v.1.4.4 (http://tree.bio.ed.ac.uk/software/Fig.tree/) and Inkscape 1.1, respectively.

The BoFADS 3D structural homology model was built using the RaptorX server.[40] The software automatically chose the FADS from CaFADS as best template (for both full length protein and each of the domains when independently taken). Confidence scores used to indicate the quality of predicted 3D models included *p*-value for the relative global quality, global distance test (GDT) and unnormalized GDT (uGDT) for the absolute global quality. Sequence conservation was projected on the BoFADS 3D structural model by the ConSurf server (https://consurf.tau.ac.il).[41] PyMol was used to visualize structures and to produce figures,[42] and the on-line server including PDB2PQR 3.1.0 and APBS 3.0.0 (https://server.poissonboltzmann.org/) was used to evaluate surface electrostatic potentials.[43]

3 | RESULTS AND DISCUSSION

3.1 | BoFADS purifies as a folded protein when overexpressed in *E. coli*

The BoFADS sequence predicted a theoretical molecular weight of 36.4 kDa, an isoelectric point of 5.96, an average hydropathicity (grand average of hydropathicity, GRAVY) of −0.174 and an instability index of 32.09. The two later parameters predicted the protein as stable in solution. SDS–PAGE confirmed that the produced enzyme was pure to homogeneity and predicted an apparent molecular weight (MW) of 36.6 kDa (Figure 2a, inset). SDS–PAGE of these samples incubated with the BS_3 cross-linker failed to show significant stabilization of oligomeric species, suggesting that under the assayed conditions, BoFADS was preferentially a monomer (Figure 2a, inset).

The UV–visible spectra of purified BoFADS showed an unusual hyperfine splitting absorption band corresponding to the absorption of aromatic side-chains

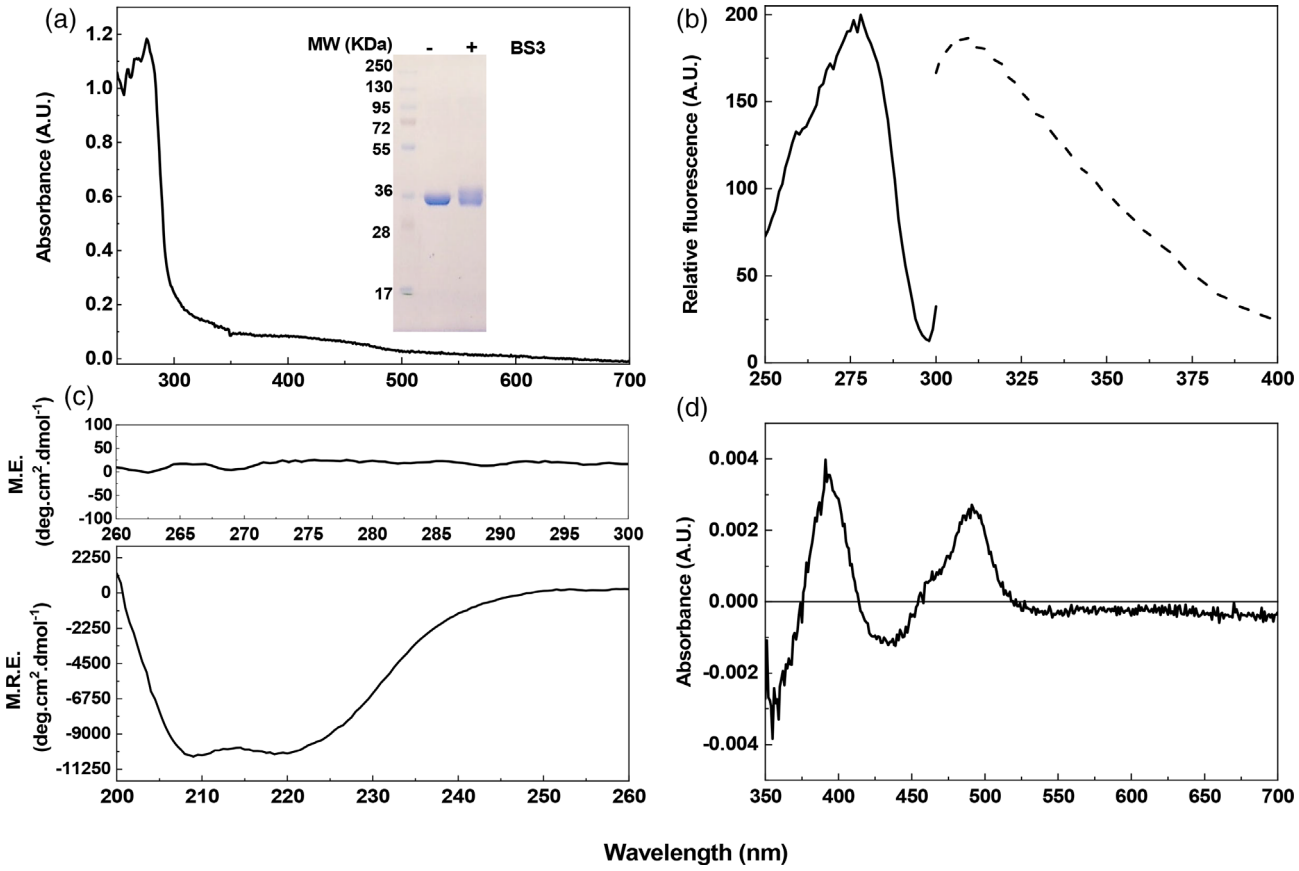

FIGURE 2 Spectroscopic properties of BoFADS. (a) UV/Vis absorption spectrum of BoFADS (125 μM). The inset shows resolution by SDS–PAGE of BoFADS as purified and after incubation with the BS_3 crosslinker. (b) Fluorescence emission spectrum of BoFADS (20 μM) (dashed line) when exciting at 280 nm, and the corresponding excitation spectrum (black continuous line) when collecting emission at 307 nm. (c) Near-UV CD (top) and far-UV CD (bottom) spectra of BoFADS (20 and 5 μM, respectively). (d) Visible difference spectrum elicited upon titration with FMN (20 μM) of a sample of BoFADS (5 μM) saturated with ADP (450 μM) and 10 mM $MgCl_2$. All spectra were recorded in 20 mM PIPES, pH 7.0 at 25 °C

with maxima at 260, 265 and 276 nm, as well as remarkable low absorptivity (Figure 2a). These features have not been observed in previously reported prokaryotic FADSs and agree with the complete absence of Trp residues in BoFADS sequence and with the remarkable high number of Phe residues, 26, versus 6 Tyr. Ten of these aromatic residues are highly conserved in other FADSs, especially the Phe residues sitting in the N terminal (*B. ovis* numbering 29, 59, 99, 111, 131, 133) (Figures S1 and S2).[4,17,18,33] As a consequence, the theoretical BoFADS absorptivity coefficient is $\varepsilon_{280nm} = 8.94\ mM^{-1}.cm^{-1}$, considerably lower than those reported for other bacterial FADSs.[4,33,44]

The fluorescence emission spectrum of BoFADS registered a maximum at 307 nm (Figure 2b), while the excitation spectrum showed a maximum at 278 nm with a shoulder at 259 nm. These features are again typical of fluorescence spectra for aromatic residues different from Trp, particularly Tyr. Also in agreement with the absence of Trp, main responsible for the near UV CD signals of proteins, the near UV CD spectrum of BoFADS hardly shows any feature (Figure 2c, top). The far-UV CD spectrum of BoFADS showed a broad negative band with minima at 209 and 218 nm (Figure 2c, bottom), revealing the presence of β-sheets and α-helices as secondary structure elements and confirming that the heterologously produced BoFADS is folded.

Finally, BoFADS yielded visible difference spectra when titrated with oxidized FMN in the presence of ADP but not in its absence (Figure 2d). These observations indicated that the ADP product of the RFK activity favors the FMN binding, suggesting that, as in other FADSs, this binding occurs at the RFK site.[5,20]

3.2 | Purified BoFADS exhibits RFK, FMNAT and FADpp activities

The ability of BoFADS to transform RF, FMN and FAD under different conditions was first qualitatively

evaluated, both in crude extracts expressing the protein as well as in purified protein solutions. Identification of the products of the RFK, FMNAT and FADpp reactions was carried out by TLC (Figure 3). In bacterial FADSs these activities can be dependent or independent on the reducing environment, as well as on the concentration of Mg^{2+}. Therefore, we carried out set of assays under different environments provided by sodium dithionite ($Na_2S_2O_4$) and concentrations of Mg^{2+}.[4,33]

When either crude extracts expressing BoFADS (Figure 3a) or the purified protein (Figure 3b) were incubated with RF and ATP consumption of the RF substrate was observed, while transformation of flavins was hardly detected in *E. coli* cells lacking the pET28a-BoFADS plasmid (Figure S3). FMN was the final product of the reaction when the reducing agent was absent, but the presence of sodium dithionite enhanced the flavin transformation up to FAD (see Figure 3a,b, lanes 2–3). Similarly, when using as substrates either FMN and ATP or FAD and PPi transformation of substrates was only produced when the reducing agent was present (see Figure 3a,b, lanes 4–5). Therefore, BoFADS, both in crude extracts and when purified to homogeneity, was able to transform RF into FMN through a RFK activity independent of the redox state of the media, whereas both the FMNAT and FADpp activities required reducing conditions.

Subsequent qualitative (TLC) and quantitative (HPLC) screenings of best performing conditions confirmed that the RFK activity was independent on the reducing agent concentration (Figures 3b and S3). In addition, Mg^{2+} was shown a requirement for the RFK activity, with cation concentration in the 0.8–10 mM range producing maximal activity (Figure S3). These conditions agree with those described in other prokaryotic FADSs, as well as in HsRFK.[3–5,33] Best catalytic conditions for the FMNAT and FADpp activities confirmed that a strong reducing environment and Mg^{2+} were

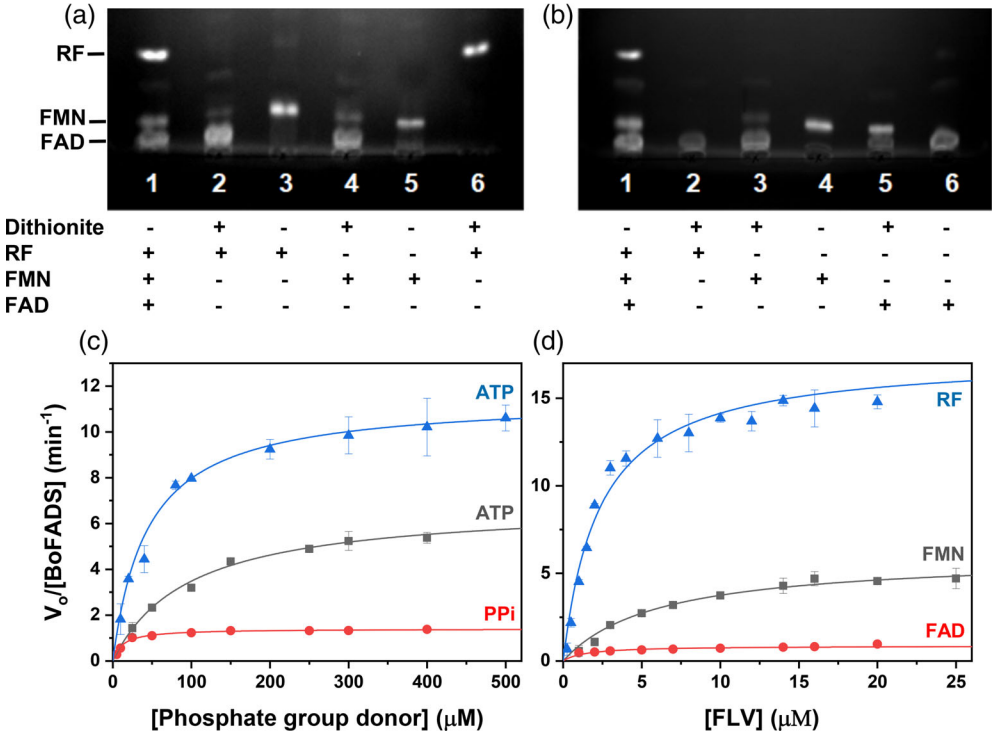

FIGURE 3 Detection of the RFK, FMNAT and FADpp activities of BoFADS. Thin layer chromatography resolution of the products of the transformation of RF, FMN and FAD by (a) crude extracts of *Escherichia coli* BL21(DE3) cells transformed with the pET28a-BoFADS plasmid and (b) purified BoFADS. Flavin transformation was evaluated under the conditions indicated in the panels regarding flavin content and presence of reducing agent (10 mM, if present). Reaction mixtures contained either 0.1 mg crude extracts or 1 μM of purified enzyme, 50 μM of the corresponding flavin and 3.5 mM ATP or PPi, in 50 mM Tris/HCl, pH 7.6, and were incubated for 15 min at 37 °C. The first lane on the left shows as control a sample containing RF, FMN and FAD (50 μM each) in same buffer. Michaelis–Menten plots as a function of variable concentrations of substrates providing (c) the phosphate group donor (ATP for RFK and FMNAT activities and PPi for FADpp activity) and (d) flavin to be transformed (FLV; RF, FMN and FAD). Reaction rates were obtained in 20 mM Tris/HCl, pH 8.0 and 1 mM and 10 mM $MgCl_2$ for the RFK (blue lines) and the FMNAT (grey lines)/FADpp (red lines) activities, respectively, including 150 mM KCl and 20 mM sodium dithionite in the case of FMNAT/FADpp activities. Mixtures were incubated 5 min at 37 °C after adding the enzyme at a final concentration of 50 nM for RFK activity and 500 nM for FMNAT/FADpp activities

required. Moreover, these activities were slightly more efficient at pH 8.0 than at 7.0, with the presence of 150 mM KCl improving their reproducibility. Therefore, herein, kinetic parameters for the FMNAT and FADpp activities were evaluated in 20 mM Tris/HCl and in the presence of sodium dithionite, pH 8.0, with 150 mM KCl, while those for the RFK activity were evaluated at both pH 7.0 and pH 8.0.

3.3 | The RFK is the most efficient activity in BoFADS

Plots of steady-state rates versus substrate concentrations for the RFK, FMNAT and FADpp activities of BoFADS showed Michaelis–Menten profiles for all substrates (Figure 3c,d), allowing determination of k_{cat} and K_M values. Table 1 summarizes the kinetic parameters for the RFK activity at pH 7.0 and 8.0. k_{cat} and K_M^{ATP} values were nearly pH-independent, but K_M^{RF} suggested RF affinity decreases when increasing pH, thus making the enzyme slightly less efficient in transforming RF at pH 8.0. Furthermore, no inhibition by excess of the RF substrate was detected. This is contrary to that reported for CaFADS,[36] but in line with previous data for other enzymes.[3,4,18,20,45] Nonetheless, when comparing k_{cat}, K_M^{RF} and K_M^{ATP} parameters among RFK activities in proteins from different organisms, the BoFADS efficiency for the transformation of RF into FMN is in a medium-low range[3–5,20] (Table 1).

k_{cat} values for the FMNAT and FADpp activities of BoFADS are, respectively, around 2-fold and up to 10-fold slower than for the RFK activity. K_M values for the FMNAT activity are suggestive of slightly weaker binding of substrates, while the corresponding values for the FADpp activity suggest stronger binding (Table 2). Noticeably, efficiency for the transformation of FMN by BoFADS shows an average value when compared with other bacterial and human FADSs, while it appears considerably less efficient regarding the second substrate, ATP. Finally, kinetic parameters for the FADpp activity of BoFADS indicate that this enzyme is more efficient in the conversion of FAD into FMN than *Homo sapiens* FADS isoform 2 (HsFADS2), the only enzyme for which parameters are available.[46] Altogether, catalytic efficiencies for the transformation of the flavin substrate indicates that under the *in vitro* assayed conditions, the phosphorylation of RF is the most efficient activity catalyzed by BoFADS, while the FADpp activity is the less efficient.

3.4 | Binding of RFK substrates in BoFADS is the kinetically preferred process during the RFK activity

We then used stopped-flow spectrophotometry to evaluate binding kinetics of flavin nucleotides involved in the RFK reaction of BoFADS, namely RF and FMN. As flavin fluorescence is modulated by the surrounding media, this

TABLE 1 Steady-state kinetic parameters for the RFK activity of BoFADS and FADSs from other bacteria, as well as of HsRFK

Enzyme	k_{cat} (min^{-1})	K_M^{ATP} (μM)	k_{cat}/K_M^{ATP} (min^{-1} μM^{-1})	K_M^{RF} (μM)	k_{cat}/K_M^{RF} (min^{-1} μM^{-1})	K_i^{RF} (μM)
BoFADS[a]	12 ± 1	50 ± 5	0.2 ± 0.1	0.6 ± 0.1	20 ± 6	
BoFADS[b]	15 ± 1	44 ± 3	0.3 ± 0.1	2.3 ± 0.3	6.5 ± 1.3	
CaFADS[c], RFK module	130 ± 30	40 ± 12	3.2 ± 1.7	6.9 ± 0.4	19 ± 5	1.9 ± 0.2
SpnFADS[d]	55 ± 2	75 ± 7	0.7 ± 0.1	1.2 ± 0.3	46 ± 13	
LmFADS-I(−)[e]	33 ± 2	41 ± 2	0.8 ± 0.1	0.5 ± 0.1	66 ± 4	
LmFADS-I(+)[e]	95 ± 7	12 ± 1	7.9 ± 1	10 ± 1	95 ± 0.8	
SaFADS[f]	25	72	0.34	8.4	3.0	
EcFADS[g]	23.4			2	11.7	
HsRFK[h]	102 ± 7	30 ± 8	3.4 ± 1.1	2.5 ± 0.4	41 ± 9	

[a]In 20 mM PIPES, pH 7.0, 1 mM $MgCl_2$ at 25 °C ($n = 3$, mean ± *SD*).
[b]In 20 mM Tris/HCl, pH 8.0, 1 mM $MgCl_2$ at 37 °C ($n = 3$, mean ± *SD*).
[c]Data from Sebastián et al.[5] In 20 mM PIPES, pH 7.0, 0.8 mM $MgCl_2$ at 25 °C.
[d]Data from Sebastián et al.[20] In 20 mM PIPES, pH 7.0, 0.8 mM $MgCl_2$ at 25 °C.
[e]Data from Sebastián et al.[4] In 20 mM PIPES and 0.8 mM $MgCl_2$, pH 7.0, at 25 °C, both in absence (−) and presence (+) of 24 mM sodium dithionite.
[f]Data from Lohithakshan et al.[18] In 50 mM Tris/HCl, pH 8.0, 10 mM $MgCl_2$, at 37 °C. Estimated errors in k_{cat} and K_M were within 10%.
[g]Data from Langer et al.[51] In 50 mM potassium phosphate, pH 7.6, 6 mM $MgCl_2$, 24 mM sodium dithionite, at 37 °C.
[h]Data from Anoz-Carbonell et al.[3] In 20 mM PIPES, pH 7.0, 0.3 mM $MgCl_2$, at 25 °C ($n = 3$, mean ± *SD*).

TABLE 2 Steady-state kinetic parameters for the FMNAT and FADpp activities of BoFADS, different prokaryotic FADSs and different isoforms of the monofunctional HsFADS

FMNAT activity					
Enzyme	k_{cat} (min^{-1})	K_M^{ATP} (μM)	k_{cat}/K_M^{ATP} (min^{-1} μM^{-1})	K_M^{FMN} (μM)	k_{cat}/K_M^{FMN} (min^{-1} μM^{-1})
BoFADS[a]	7.0 ± 0.3	97 ± 9	0.07 ± 0.01	5.1 ± 0.4	1.4 ± 0.2
CaFADS[b]	39 ± 1	43 ± 8	0.9 ± 0.2	6 ± 1	6 ± 1
SpnFADS[c]	34.9	31.6	0.7	9.8	3.6
LmFADS-I(+)[d]	108 ± 8	215 ± 15	0.5 ± 0.1	42 ± 3	2.6 ± 0.2
LmFADS-II(−)[d]	65 ± 5	7.4 ± 0.6	8.8 ± 0.8	55 ± 5	1.2 ± 0.2
LmFADS-II(+)[d]	43 ± 3	37 ± 2	2.0 ± 0.2	71 ± 6	0.6 ± 0.1
SaFADS[e]	9.1	77	0.12	5.1	1.8
EcFADS[f]	3.6			4.0	0.9
HsFADS1[g]	0.30 ± 0.08			1.3 ± 0.7	0.23 ± 0.18
HsFADS2[h]	4.7 ± 0.2	15 ± 2	0.30 ± 0.05	0.35 ± 0.10	13.4 ± 4.4
FADpp activity					
Enzyme	k_{cat} (min^{-1})	K_M^{PPi} (μM)	k_{cat}/K_M^{PPi} (min^{-1} μM^{-1})	K_M^{FAD} (μM)	k_{cat}/K_M^{FAD} (min^{-1} μM^{-1})
BoFADS[a]	1.4 ± 0.1	12 ± 2	0.12 ± 0.03	1.5 ± 0.5	0.9 ± 0.36
HsFADS2[h]	0.31 ± 0.02			82 ± 2	$(3.8 \pm 0.3)\cdot 10^{-3}$

[a]In 20 mM Tris/HCl, pH 8.0, 10 mM $MgCl_2$, 0.15 mM KCl, 20 mM sodium dithionite at 37 °C ($n = 3$, mean ± SD).
[b]Data from Serrano et al.[44] In 20 mM PIPES, pH 7.0, 10 mM $MgCl_2$ at 25 °C.
[c]Data from Sebastián et al.[33] In 20 mM PIPES, pH 7.0, 0.8 mM $MgCl_2$, 3 mM sodium dithionite at 25 °C. Estimated errors in k_{cat} and K_M are within ±10%.
[d]Data from Sebastián et al.[4] In 20 mM PIPES, pH 7.0, 0.8 mM $MgCl_2$, both in absence (−) and presence (+) of 24 mM sodium dithionite at 25 °C.
[e]Data from Lohithakshan et al.[18] In 50 mM Tris/HCl, pH 8.0, 10 mM $MgCl_2$, 24 mM sodium dithionite at 37 °C. Estimated errors in k_{cat} and K_M were within 10%.
[f]Data from Langer et al.[51] In 50 mM potassium phosphate, pH 7.6, 6 mM $MgCl_2$ at 37 °C.
[g]Data from Torchetti et al.[52] In 50 mM Tris/HCl, pH 7.5, 5 mM $MgCl_2$ at 37 °C.
[h]Data from Torchetti et al.[46] In 50 mM Tris/HCl, pH 7.6, 5 mM $MgCl_2$ at 37 °C.

technique allows detecting small changes in the flavin isoalloxazine environment due to its binding/dissociation or to protein conformational rearrangement. Meanwhile, RF transformation into FMN is not observed due to the same fluorescence spectra and yields of both flavins.[5,20] When mixing BoFADS with FLV ligands observed fluorescence decays were very slow and decreased with ligand concentration, being therefore suggestive of only flavin photobleaching taking place. Therefore, BoFADS does not appear to internalize by itself the FLV ligands in the expected catalytically competent entrapped conformation. This observation is similar to that reported in monofunctional eukaryotic RFKs and RFK modules of FADSs from other species.[3,5,20]

Nonetheless, when mixing BoFADS with different combinations of ANP and FLV ligands, an exponential decay in fluorescence was detected in the 8 s time frame (Figure 4a). We related this fluorescence decay to FLV binding and/or entrapment within the protein matrix (Figure 4c).[3,5,20] This made us to conclude that the presence of ANP induces the capability of the RFK site of BoFADS to entrap the isoalloxazine ring of the FLV ligand.[5] Binding of the RF–ATP substrates showed the largest decay in amplitude of the signal. Binding of the FMN–ADP (products) or RF–ADP combinations produced decays with amplitudes half of that of RF–ATP substrates. Finally, the FMN–ATP combination showed very minor amplitude for the decay that suggests entrapment of FMN is hardly occurring. These observations indicate that binding of substrates is favored in number of molecules over the binding of other combinations of ligands. After the initial decay, those samples containing RF with ANP showed a subsequent recover in flavin fluorescence. Such a feature was previously related to reopening of the flavin binding site, making the isoalloxazine again solvent accessible.[5,20]

Noticeably, this overall behavior of BoFADS slightly differed from the ones reported when similarly evaluating other family members.[3,5,20] In fact, profiles for the BoFADS initial decays are in a manner more similar to those reported for the RFK site of SpnFADS than to those of HsRFK and CaFADS.[3,5,20] Moreover, the BoFADS behavior also differs regarding the FLV fluorescence recover, previously related to the ATP presence for

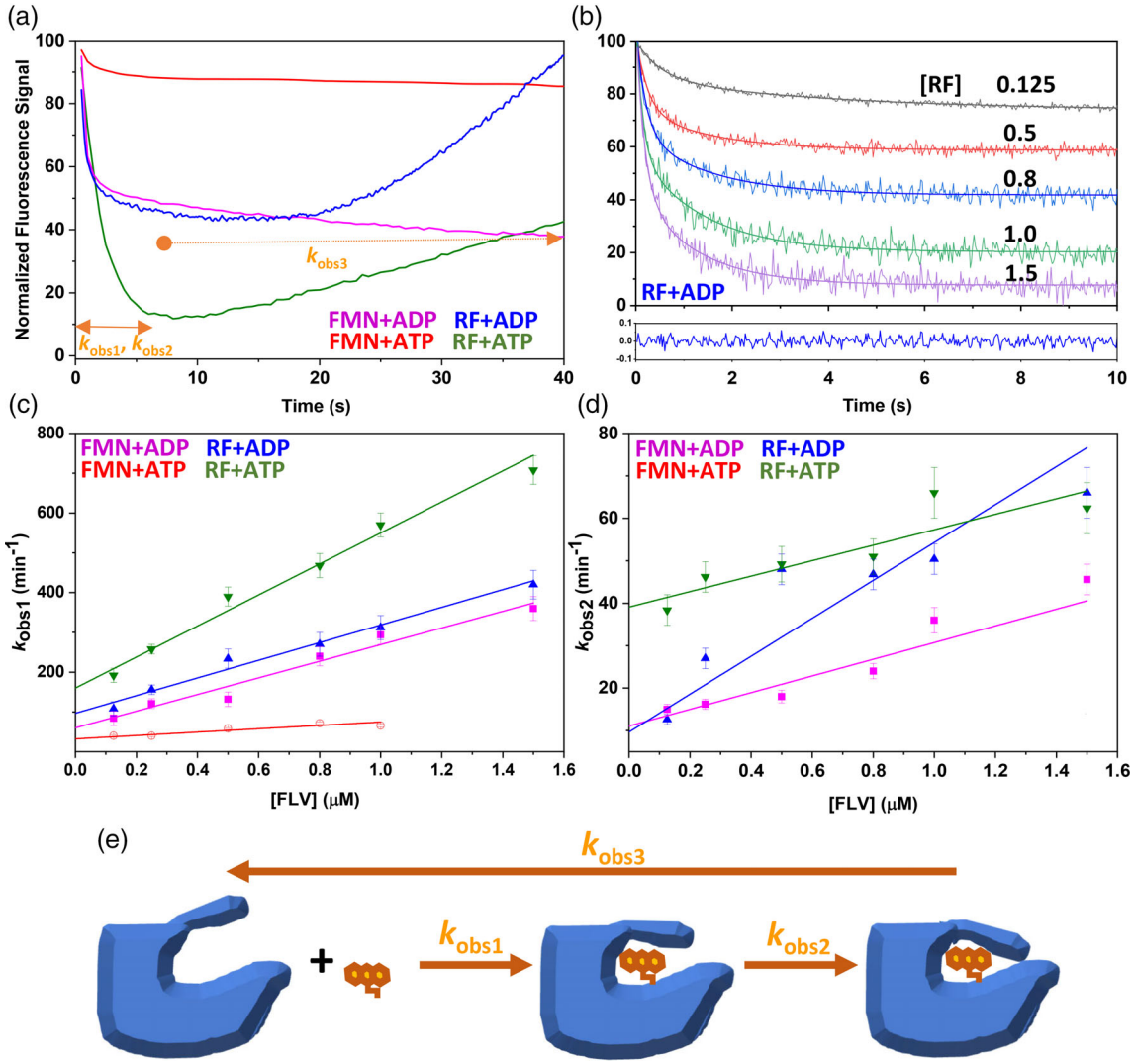

FIGURE 4 Pre-steady-state stopped-flow kinetics of the binding of RF and FMN to the RFK site of BoFADS in the presence of adenine nucleotides. (a) Normalized evolution of kinetic changes in fluorescence upon mixing BoFADS (0.2 μM) with all possible FLV-ANP ligand combinations (0.8 and 250 μM, respectively). (b) Example of the fittings of kinetic traces corresponding to mixtures of BoFADS with RF-ADP, and residuals of the fitting of the 0.8 μM RF–250 μM ADP data to a biexponential function. Evolution of (c) k_{obs1} and (d) k_{obs2} as a function of the FLV concentration. All measurements were carried out in 20 mM PIPES, pH 7.0, 0.8 mM $MgCl_2$ and 0.3 mM NaCl at 25 °C. (e) Scheme representing the processes corresponding to different steps in FLV accessibility to the solvent

CaFADS and SpnFADS: the cavity re-opening in BoFADS appears rather related to the RF substrate binding, whereas binding of FMN prevents it. This suggests that RF entrapment induces a rearrangement in the FLV site that subsequently triggers the mechanism to bring the isoalloxazine ring back to the solvent. Noticeably, in the case of HsRFK no recovering of flavin fluorescence was observed.[3] Such differences can be related to conformational changes at the RFK domain of prokaryotic FADSs for ligand binding and product release being more complex than for monofunctional eukaryotic RFKs, as well as to a role of the RFK domain modulating the activity of the FMNAT domain upon production of transient quaternary organizations during catalysis.[47] Therefore, species-specific traits are found in BoFADS for FLV entrapment and release at the RFK site.

Fitting analysis of the initial decays related to FLV binding to the RFK site of BoFADS also revealed kinetic differences. A single exponential decay best fits to traces for the FMN–ATP ligand combination. However, two independent exponentials are required to describe the binding kinetics for the RF–ANP and FMN–ADP mixtures (Figure 4b), with the amplitude (A_1) of the first process dominating the fluorescence decay ($A_2 < 10\%A_1$). These observations suggest the potential presence of two conformational states for FLV entrapment. We identified the initial process as FLV binding/entrapment at the RFK site of BoFADS by displacement of loop FlapII (see

below), similarly to that reported for other family members.[3,5,20] The succeeding fluorescence decay must relate to subsequent conformational changes in the BoFADS loops contributing to further entrapment of the isoalloxazine ring after the initial binding.

The k_{obs1} values from these fittings showed a linear dependence on the FLV concentration (Figure 4c), with rates for the binding of substrates of the reaction at saturating concentrations nearly twice faster than for FLV–ADP ligands. These data allowed determining k_{on} and k_{off} for FLV binding, as well as the dissociation constant (K_d) and free energy (ΔG) of the process (Table 3). These data indicated that binding processes containing the RF and ATP substrates are the fastest and produce the largest changes in fluorescence decay amplitude (Figure 4a). Therefore, the RFK site of BoFADS binds preferably the substrates of the RFK reaction over other combinations of ligands, similarly to SpnFADS and HsRFK but contrary to CaFADS. Noticeably, binding of the FMN product in presence of ATP was the less favored process from the kinetic viewpoint (smaller k_{on}) and number of FMN molecules entrapped, while the combination of FMN–ADP products and RF–ADP showed half of amplitude of that of substrates as well as k_{on} values. k_{off} values follow similar traits. Finally, the thermodynamic parameters derived from k_{on} and k_{off}, indicated that, regarding affinity, BoFADS binds the products of its activity, FMN and ADP, slightly stronger than the RF–ANP combinations, while FMN–ATP is the less stable association (Table 3).

When detected, k_{obs2} also showed a linear dependence on the FLV concentration (Figure 4d), allowing to derivate kinetic and thermodynamic parameters of a putative reorganization step (Table 3). These data indicate that reorganization is faster and stronger for FLV–ADP combinations than for the substrates one, suggesting that this process is more relevant for the binding of combinations of ligands noncompetent for catalysis. Interestingly, $k_{off\text{-}reg}$ values for the RF–ATP substrates is substantially faster than for FLV–ADP combinations, while values for the FLV–ADP ones are situated in the k_{cat} range (Tables 1 and 3). Collectively, these observations indicate that kinetics of release of nonproductive ligands, including products, might limit the RFK catalytic activity of BoFADS.

Altogether, our results indicate that the presence of ANP is necessary for RF entrapment in BoFADS and that the binding of substrates of the RFK activity (RF and ATP) is the fastest process and the one occurring in a major number of molecules.

3.5 | Subtle primary and ternary structural traits are behind regulation of activities in prokaryotic FADSs

Kinetics and binding studies have envisaged species-specific conformational changes along the catalytic cycles of FADSs from different organisms. However, to the date they are not proven at the molecular level because crystal structures are only available for CaFADS (PDB 2X0K) and SpnFADS (PDB 3OP1).[22,48] This makes worthy to evaluate sequence divergence and evolution within the FADS family members.

Multiple sequence alignments provide a couple of interesting observations. First, only a few key residues appear conserved in nearly all the 42 prokaryotic FADSs from different bacterial phyla and classes here evaluated (Figures 5, S1 and S2). Second, Trp residues appear rare as constituents of these FADSs and, when present, they are hardly conserved in alignments, contrary to that observed for Phe residues (Figures S1and S2). Our phylogenetic analysis shows that proteins from the *Mycoplasma* genus root the tree (bootstrap >93), clearly diverging from the rest (Table S1 and Figure 6). Two other clades separate from the one that includes the remaining 30 FADSs. One of the divergent clades (bootstrap >92) groups FADSs from the *B. subtilis*, *S. aureus*, *L. monocytogenes*, *S. pneumoniae*, *E. faecium* and

TABLE 3 Pre-steady-state kinetic parameters for the binding and dissociation of flavins to the RFK site of BoFADS in the presence of adenine nucleotides

Ligand combination	k_{obs1} (initial flavin binding)				k_{obs2} (further flavin entrapment)			
	k_{on} (min^{-1} μM^{-1})	k_{off} (min^{-1})	K_d (μM)	ΔG (kcal mol^{-1})	$k_{on\text{-}reg}$ (min^{-1} μM^{-1})	$k_{off\text{-}reg}$ (min^{-1})	$K_{d\text{-}reg}$ (μM)	ΔG_{reg} (kcal mol^{-1})
RF–ATP	390 ± 24	160 ± 13	0.41 ± 0.06	−8.7 ± 0.1	18 ± 1	39 ± 1	2.2 ± 0.2	−7.7 ± 0.1
RF–ADP	222 ± 17	97 ± 9	0.44 ± 0.07	−8.6 ± 0.1	44 ± 1	10 ± 1	0.23 ± 0.03	−9.0 ± 0.1
FMN–ATP	42 ± 9	32 ± 5	0.76 ± 0.28	−8.3 ± 0.2	–[a]	–[a]	–[a]	–[a]
FMN–ADP	210 ± 23	60 ± 14	0.29 ± 0.10	−8.9 ± 0.2	20 ± 1	11 ± 1	0.55 ± 0.08	−8.5 ± 0.1

Note: Experiments were performed in 20 mM PIPES, pH 7.0, 0.8 mM $MgCl_2$ at 25°C ($n = 5$, mean ± *SD*) in a stopped-flow equipment.
[a]Process not observed for this combination of ligands.

L. plantarum bacilli and from the *C. trachomatis* chlamydia, while the other (bootstrap >52) groups the enzymes from the spirochaete *T. denticola* and the firmicute *A. thermocellus*. The remaining 30 sequences clade together and include BoFADS, FADSs from most ESKAPE pathogens (which subclade together with the single exception of *E. faecium*), as well as CaFADS. Despite this clade is formed by several subclades, their low bootstrap values suggest that these FADSs are relatively conserved regarding evolution. Nonetheless, as expected, BoFADS appears more closely related to FADSs from other alphaproteobacteria. Plotting residue conservation on the homology model built for BoFADS particularly shows that conserved motifs and conserved

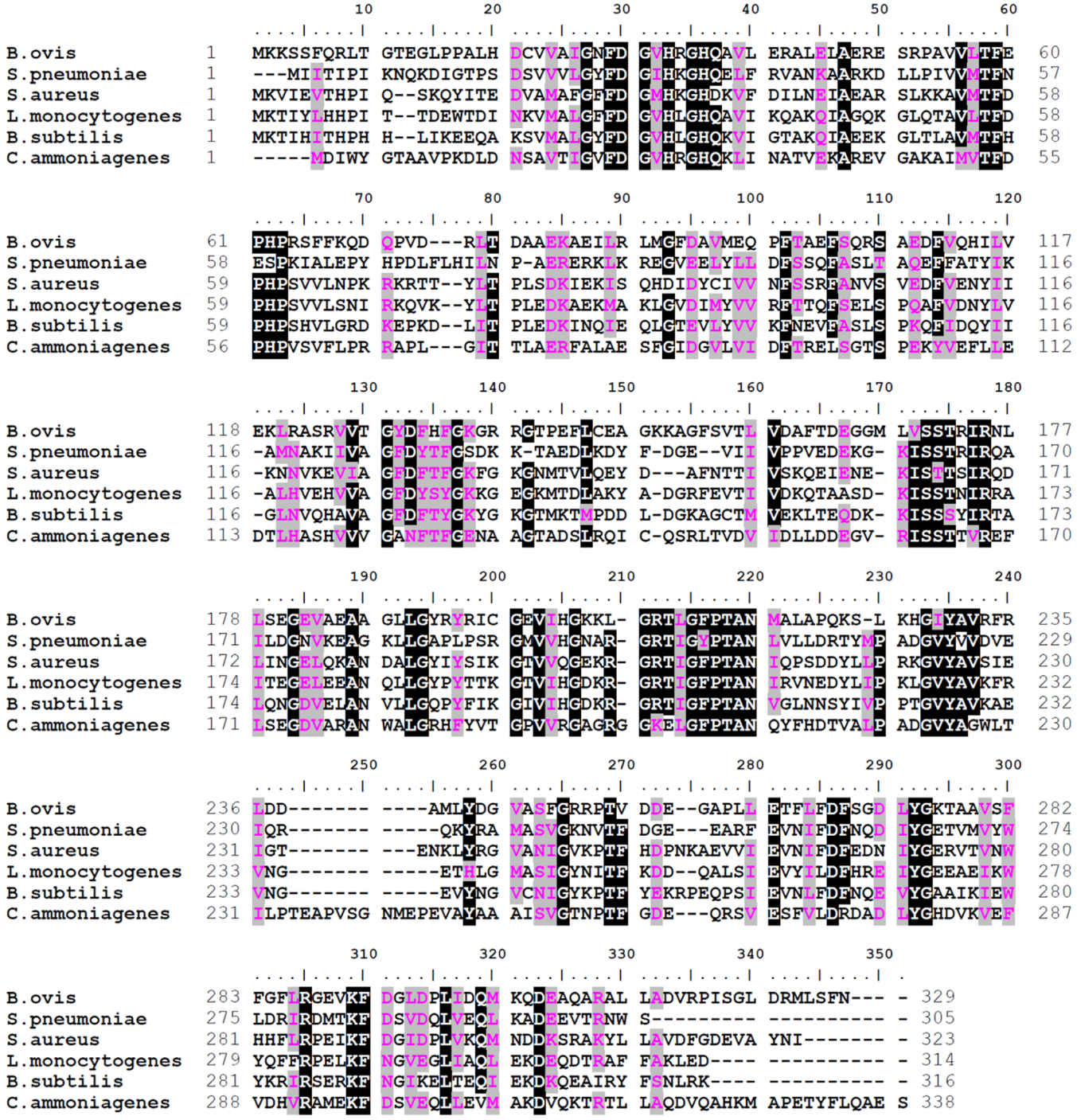

FIGURE 5 Multiple sequence alignment of BoFADS, SpnFADS, SaFADS, LmFADS-I, BsFADS and CaFADS. The alignment was constructed with Clustal Omega. Regions with identical residues are highlighted in black with residues in white. Residues showing conservative substitutions over 75% are shown in red purple and highlighted in grey

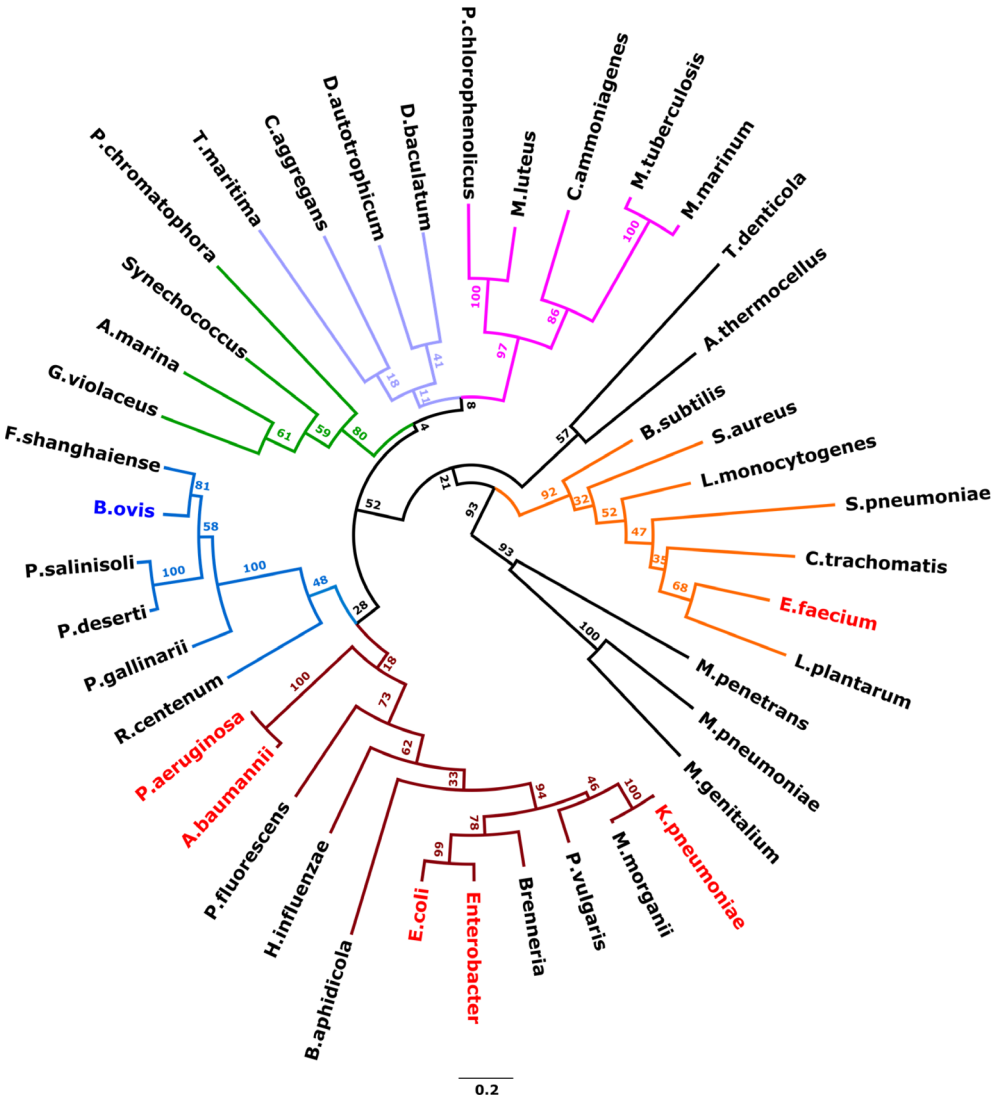

FIGURE 6 Phylogeny of selected bacterial FADSs. The evolutionary history was inferred by using the maximum likelihood method and JTT matrix-based model with MEGA X. The tree with most likelihood (−15474.59) is shown. The analysis involved 42 FADS sequences (Table S1). FADSs from *Mycoplasma* species (*penetrans*, *pneumoniae* and *genitalium*) highlight the evolutionary separation between clusters. ESKAPE pathogens (*Enterococcus faecium*, *Staphylococcus aureus*, *Klebsiella pneumoniae*, *Acinetobacter baumannii*, *Pseudomonas aeruginosa* and *Enterobacter* spp.), being the leading cause of nosocomial infections throughout the world, are highlighted in bold red, while *B. ovis* is highlighted in green. The percentage of trees in which the associated taxa clustered together is shown next to the branch points. The scale reflects the evolutionary distance, corresponding to 0.2 amino acid substitution per site. Main clades are highlighted with different colors

scattered residues accumulate at the binding sites of substrates for both RFK and FMNAT activities, and, particularly at the catalytic sites (Figure 7a).

At the FMNAT site the highly conserved HxGH and SSTxxIR motifs accommodate the adenine and phosphate moieties of the ATP, while the FMN isoalloxazine binding site is made by conserved scattered residues, particularly Phe (Figure 7b). Residue conservation is stronger at the ATP binding site than at the isoalloxazine binding site. The catalytic FMNAT residue is of acidic nature in most FADSs, being an Asp, D130, in BoFADS, but it is an Asn, N125, in CaFADS[49] (Figures 7b, S1, and S2). Noticeably, geometric profiles of the FMNAT binding sites and electrostatic potentials, both at the ligand binding sites and at the protein surface, considerably diverge among BoFADS, CaFADS and SpnFADS, showing more differences at the FMN binding cavity and in CaFADS (Figure 7d). This agrees with the differences in their theoretical isoelectric points (4.8, 5.4 and 5.9 for CaFADS, SpnFADS and BoFADS, respectively), but also with their experimental behaviors. Thus, reducing conditions for FMNAT and FADpp activities are required by canonical (known as FADSs of type I) BoFADS, LmFADS-I, SpnFADS, BsFADS and SaFADS, meanwhile only in the also canonical CaFADS (showing the most divergent structural and functional properties) and the LmFADS of type II (that contains the prokaryotic FMNAT domain but lacks the RFK one) such transformation is independent on the redox state of the media (Table 2).[4,45,49,50] Since the flavin substrate geometry and charge distribution differ in its reduced or oxidized state, such predicted varieties in cavity volumes, geometries and nature of residues shaping the binding sites of ligands will surely contribute to the preference of each FMNAT site for a particular redox state of its flavin substrate.[4,33,47]

At the RFK site, the active site itself concentrates most conserved residues (Figure 7c). It includes (a) the PTAN motif accommodating the phosphates of the ATP

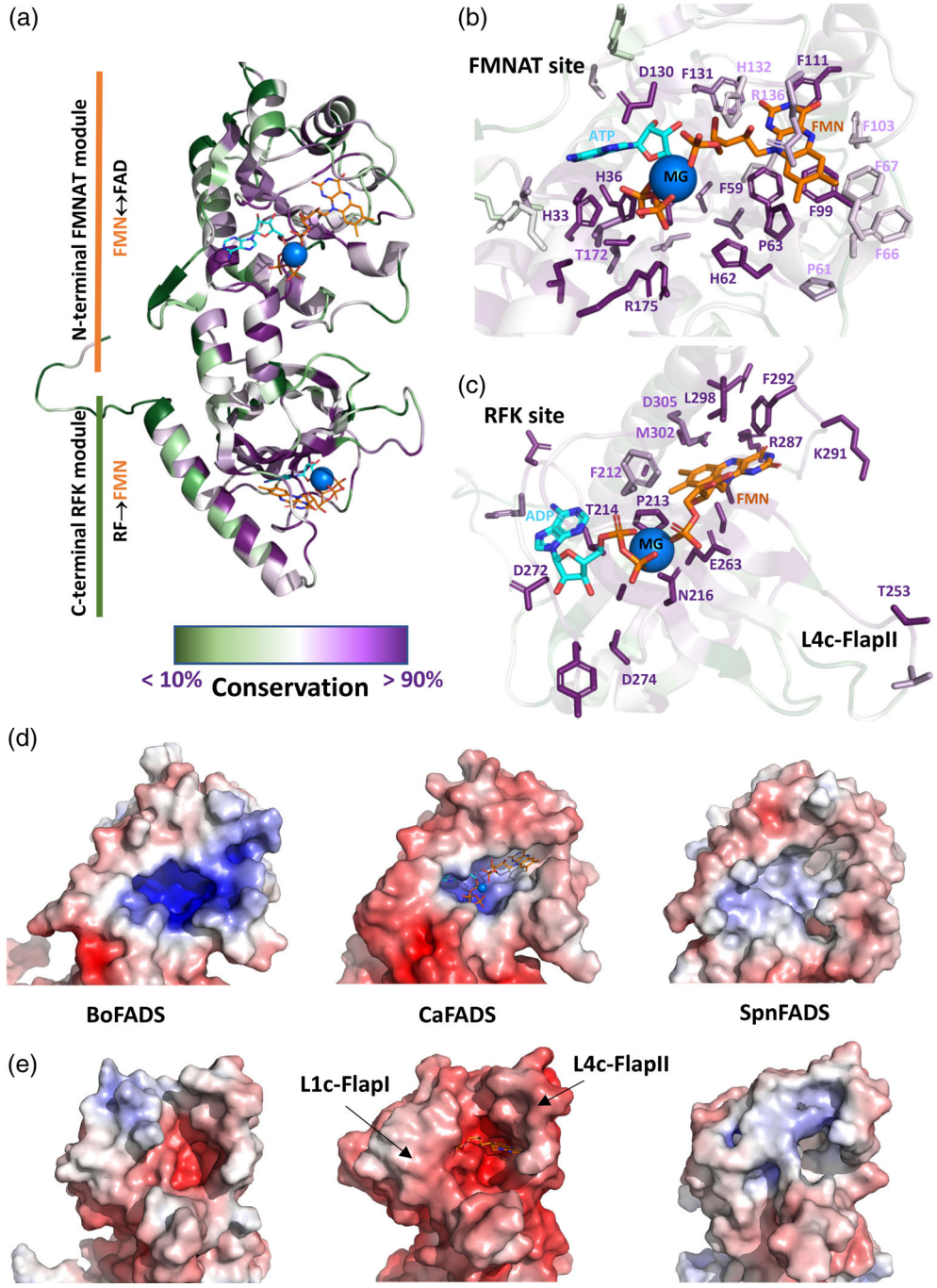

FIGURE 7 Structural conserved motifs in prokaryotic FADSs. (a) Cartoon representation of the structural model of BoFADS colored by sequence conservation in family members (Figure S1). The model was produced by homology using the RaptorX server with the BoFADS sequence as input, the server automatically chose the crystal structure of CaFADS (particularly of a R66A variant, PDB ID 4UZE_A) as template (*p*-value 1.4×10^{-11}; overall uGDT (GDT): 229 (69); 329 (100%)). Conservation score of individual amino acids was calculated on the BoFADS structural model by the ConSurf server, using as input the BoFADS model and the multiple sequence alignment of FADSs shown in Figure S1, and color represented with PyMol. Regions for the FMNAT/FADpp- and RFK-modules of BoFADS are highlighted on the left by orange and green bars respectively and corresponding transformation of flavins in each one of them indicated. Detail of residue conservation on the 3D BoFADS model for the (b) FMNAT/FADpp and (c) RFK active sites. Color legend for conservation score is shown at bottom of panel (a). Relevant residues are shown in sticks and labeled. Surface electrostatic potential distributions at the (d) FMNAT and (e) RFK active sites of the structural model for free BoFADS and the crystal structures of free CaFADS and SpnFADS. Electrostatic potential values are shown on a scale from red to blue, corresponding to −10.0 and +10.0 kT/e, respectively, at 298 K. In some panels, ligands at active sites are modeled and shown in sticks with carbon in light blue and orange, respectively, for adenine and flavin nucleotides, while Mg^{2+} ions are shown as blue spheres. Substrates (ATP, FMN and Mg^{2+}) at the FMNAT site have been modeled based on an reported energetically optimized interaction model for CaFADS,[47] while products (ADP, FMN and Mg^{2+}) at the RFK site have been allocated base on the crystal structure of the ternary CaFADS:FMN:ADP:Mg^{2+} complex (PDB ID: 5A89[22])

substrate and the Mg^{2+} cation bridging them, as well as (b) the Glu catalytic residue: E268 in CaFADS and E263 in BoFADS (Figures 7c and S2). The GGRRxx(L/I) residues that precede the PTAN motif form a flexible loop, known as FlapI (L1c), that accommodates the adenine moiety of the ATP/ADP nucleotide. Some scattered conserved residues are also found in FlapII (L4c), a long protein flexible loop that entraps the flavin ring during the RFK catalytic cycle.[22] The conformational rearrangement of FlapII has been demonstrated in ternary complexes of CaFADS and HsRFK, and observed when similarly evaluating binding of flavins to other FADSs, including BoFADS (Figure 4).[2,5,20,22] In the free CaFADS structure the PTAN motif and FlapI occupy the RFK site of phosphates and adenine of the ATP substrate, respectively. Rearrangements of these elements upon concerted ligand binding have been shown as key in substrates association and products dissociation during RFK catalysis. Despite sequence conservation in these motifs, in FADSs different from CaFADS these conformational changes at PTAN and FlapI are not required, as exemplified by the SpnFADS structure (PDB: 3OP1), being these enzymes ready for ATP:Mg^{2+} binding and stabilisation.[20,22] Moreover, inhibition of the RFK activity by the RF substrate has only been reported in CaFADS, relating the changes in conformation at its PTAN and FlapI regions with this additional mechanism for activity regulation.[3,5,20] Kinetics of flavin binding at the RFK site also identify differences in flavin entrapment mechanisms.[3,5,20] In HsRFK, SpnFADS and BoFADS, binding of substrates of the RFK reaction—RF and ATP—is kinetically favored (Table 3),[3,20] while any other combination of ligands is faster in CaFADS.[5]

Noticeably, one of the main divergences at the RFK site relates to flavin release after catalysis. While for some enzymes the ATP substrate is the one apparently triggering the subsequent release process, in BoFADS this role appears to be carried out by RF. Moreover, in HsRFK dissociation of products is by far the limiting step during catalysis and the presence of the client apo-protein appears required to liberate the flavin from its entrapment.[3,5,20] When evaluating crystal structures showing flavin entrapment at the RFK site, namely ternary complexes for CaFADS and HsRFK, it is observed that the closed conformations of FlapII are stabilized by the interaction not only with the flavin ligand, but also with FlapI and other structural elements at the edge of the binding cavity. Therefore, displacement of FlapII must induce a reorganization of the RFK module, or vice versa, but particularly of the catalytic and flavin binding sites, as well as of the electrostatic environment of ligands. Noticeably, meanwhile the FlapII first midportion shows some conservation among the FADSs evaluated, its second portion is highly divergent regarding amino acid content and predicted electrostatic distribution (Figures 7c,e and S2). In fact, it is worth to note that the surface electrostatic potential, both at ligands binding sites and in the overall surface, considerably differs among the RFK domains of the compared proteins. This might suggest different relationships in the interplay of FlapII with the edge of the binding cavity during flavin entrapment, as well as in the nature itself of the catalytic and the isoalloxazine sites. Such variability in environments during flavin entrapment will surely differentiate the mechanisms involved in products release upon catalysis.

In conclusion, the characterization of the BoFADS activities and evaluation of their particular features in the context of sequence and structural conservation within bifunctional FADSs reinforces the fact that species-specific traits modulate prokaryotic RFK and FMNAT activities. This study particularly points to differences in moderately conserved and nonconserved regions and residues as having a relevant impact in substrate binding and product dissociation, and therefore on catalysis. From the so far characterized FADSs, CaFADS keeps as the most divergent, being the single one that does not require reductive environments for FMNAT catalysis, shows RF substrate inhibition and stabilizes a dimer-of-trimers during RFK catalysis. In this context, despite common mechanisms apply to FADS activities from different species, subtle changes at the substrate binding cavities and sequence divergence in connecting loops and surface protein charge, are also envisaged to specifically modulate substrates/products binding modes, and consequently, catalytic efficiencies in different family members.

ACKNOWLEDGMENTS

This research was supported by the Spanish Ministry of Science and Innovation – State Research Agency (Grant No. PID2019-103901GB-I00) and the Government of Aragón-FEDER (Grupo de Referencia Biología Estructural [E35_20R]). Authors would like to acknowledge the use of Servicios Generales de Apoyo a la Investigación-SAI, Universidad de Zaragoza. The funders had no role in the design of the study; in the collection, analyses, or interpretation of data; in the writing of the manuscript; or in the decision to publish the results.

CONFLICT OF INTEREST

The authors declare no potential conflict of interest

AUTHOR CONTRIBUTIONS

Conceptualization: Milagros Medina. *Methodology*: Marta Martínez-Júlvez, Andrea Moreno, Victor Taleb, Ernesto Anoz-Carbonell and Milagros Medina. *Formal analysis*:

Marta Martínez-Júlvez, Andrea Moreno, Victor Taleb and Milagros Medina. Investigation: Marta Martínez-Júlvez, Andrea Moreno, Victor Taleb, Ernesto Anoz-Carbonell and Milagros Medina. Data curation: Marta Martínez-Júlvez, Andrea Moreno, Victor Taleb and Milagros Medina. *Writing – original draft preparation*: Marta Martínez-Júlvez and Milagros Medina. *Writing – review and editing*: Marta Martínez-Júlvez and Milagros Medina. *Project administration*: Milagros Medina. *Funding acquisition*: Milagros Medina.

ORCID

Andrea Moreno https://orcid.org/0000-0002-5535-2762
Victor Taleb https://orcid.org/0000-0001-9224-5854
María Sebastián https://orcid.org/0000-0001-7202-4587
Ernesto Anoz-Carbonell https://orcid.org/0000-0002-6649-9153
Marta Martínez-Júlvez https://orcid.org/0000-0001-9047-0046
Milagros Medina https://orcid.org/0000-0001-8743-0182

REFERENCES

1. Karthikeyan S, Zhou Q, Mseeh F, Grishin NV, Osterman AL, Zhang H. Crystal structure of human riboflavin kinase reveals a beta barrel fold and a novel active site arch. Structure. 2003; 11:265–273.
2. Karthikeyan S, Zhou Q, Osterman AL, Zhang H. Ligand binding-induced conformational changes in riboflavin kinase: Structural basis for the ordered mechanism. Biochemistry. 2003;42:12532–12538.
3. Anoz-Carbonell E, Rivero M, Polo V, Velázquez-Campoy A, Medina M. Human riboflavin kinase: Species-specific traits in the biosynthesis of the FMN cofactor. FASEB J. 2020;34:10871–10886.
4. Sebastián M, Arilla-Luna S, Bellalou J, Yruela I, Medina M. The biosynthesis of flavin cofactors in *Listeria monocytogenes*. J Mol Biol. 2019;431:2762–2776.
5. Sebastián M, Serrano A, Velázquez-Campoy A, Medina M. Kinetics and thermodynamics of the protein–ligand interactions in the riboflavin kinase activity of the FAD synthetase from *Corynebacterium ammoniagenes*. Sci Rep. 2017;7:7281.
6. Barile M, Giancaspero TA, Brizio C, et al. Biosynthesis of flavin cofactors in man: Implications in health and disease. Curr Pharm Des. 2013;19:2649–2675.
7. Walsh CT, Wencewicz TA. Flavoenzymes: Versatile catalysts in biosynthetic pathways. Nat Prod Rep. 2013;30:175–200.
8. Macheroux P, Kappes B, Ealick SE. Flavogenomics—A genomic and structural view of flavin-dependent proteins. FEBS J. 2011;278:2625–2634.
9. Massey V. The chemical and biological versatility of riboflavin. Biochem Soc Trans. 2000;28:283–296.
10. Fraaije MW, Mattevi A. Flavoenzymes: Diverse catalysts with recurrent features. Trends Biochem Sci. 2000;25:126–132.
11. Leys D, Scrutton NS. Sweating the assets of flavin cofactors: New insight of chemical versatility from knowledge of structure and mechanism. Curr Opin Struct Biol. 2016;41:19–26.
12. Yazdanpanah B, Wiegmann K, Tchikov V, et al. Riboflavin kinase couples TNF receptor 1 to NADPH oxidase. Nature. 2009;460:1159–1163.
13. Hirano G, Izumi H, Yasuniwa Y, et al. Involvement of riboflavin kinase expression in cellular sensitivity against cisplatin. Int J Oncol. 2011;38:893–902.
14. García-Angulo VA. Overlapping riboflavin supply pathways in bacteria. Crit Rev Microbiol. 2017;43:196–209.
15. Matern A, Pedrolli D, Großhennig S, Johansson J, Mack M. Uptake and metabolism of antibiotics roseoflavin and 8-demethyl-8-aminoriboflavin in riboflavin-auxotrophic *Listeria monocytogenes*. J Bacteriol. 2016;198:3233–3243.
16. Gutiérrez-Preciado A, Torres AG, Merino E, Bonomi HR, Goldbaum FA, García-Angulo VA. Extensive identification of bacterial riboflavin transporters and their distribution across bacterial species. PLoS One. 2015;10:e0126124.
17. Herguedas B, Martinez-Julvez M, Frago S, Medina M, Hermoso JA. Oligomeric state in the crystal structure of modular FAD synthetase provides insights into its sequential catalysis in prokaryotes. J Mol Biol. 2010;400:218–230.
18. Lohithakshan A, Narayanasamy R, Potteth US, et al. Molecular insights into the mechanism of substrate binding and catalysis of bifunctional FAD synthetase from *Staphylococcus aureus*. Biochimie. 2021;182:217–227.
19. Leone P, Galluccio M, Brizio C, et al. The hidden side of the human FAD synthase 2. Int J Biol Macromol. 2019;138:986–995.
20. Sebastián M, Velázquez-Campoy A, Medina M. The RFK catalytic cycle of the pathogen *Streptococcus pneumoniae* shows species-specific features in prokaryotic FMN synthesis. J Enzyme Inhib Med Chem. 2018;33:842–849.
21. Marcuello C, Arilla-Luna S, Medina M, Lostao A. Atomic force microscopy reveals a dimer of trimers organization in *Corynebacterium ammoniagenes* FAD synthetase. FEBS J. 2012;279: 513–514.
22. Herguedas B, Lans I, Sebastián M, Hermoso JA, Martínez-Júlvez M, Medina M. Structural insights into the synthesis of FMN in prokaryotic organisms. Acta Crystallogr D Biol Crystallogr. 2015;71:2526–2542.
23. Lans I, Anoz-Carbonell E, Palacio-Rodríguez K, Aínsa JA, Medina M, Cossio P. In silico discovery and biological validation of ligands of FAD synthase, a promising new antimicrobial target. PLoS Comput Biol. 2020;16:e1007898.
24. Sebastián M, Anoz-Carbonell E, Gracia B, et al. Discovery of antimicrobial compounds targeting bacterial type FAD synthetases. J Enzyme Inhib Med Chem. 2018;33:241–254.
25. Picard-Hagen N, Berthelot X, Champion JL, et al. Contagious epididymitis due to *Brucella ovis*: Relationship between sexual function, serology and bacterial shedding in semen. BMC Vet Res. 2015;11:125.
26. De Massis F, Zilli K, Di Donato G, et al. Distribution of *Brucella* field strains isolated from livestock, wildlife populations, and humans in Italy from 2007 to 2015. PLoS One. 2019;14: e0213689.
27. OIE. Ovine epididymitis (*Brucella ovis*). Terrestrial Animal Health Code; 2019.
28. Wang Y, Ke Y, Duan C, et al. A small non-coding RNA facilitates *Brucella melitensis* intracellular survival by regulating the expression of virulence factor. Int J Med Microbiol. 2019;309: 225–231.

29. Spellerberg B, Cundell DR, Sandros J, et al. Pyruvate oxidase, as a determinant of virulence in *Streptococcus pneumoniae*. Mol Microbiol. 1996;19:803–813.
30. Tsolis RM, Seshadri R, Santos RL, et al. Genome degradation in *Brucella ovis* corresponds with narrowing of its host range and tissue tropism. PLoS One. 2009;4:e5519.
31. McNeil MB, Hampton HG, Hards KJ, Watson BN, Cook GM, Fineran PC. The succinate dehydrogenase assembly factor, SdhE, is required for the flavinylation and activation of fumarate reductase in bacteria. FEBS Lett. 2014;588:414–421.
32. Zhong Q, Kobe B, Kappler U. Molybdenum enzymes and how they support virulence in pathogenic bacteria. Front Microbiol. 2020;11:615860.
33. Sebastian M, Lira-Navarrete E, Serrano A, et al. The FAD synthetase from the human pathogen *Streptococcus pneumoniae*: A bifunctional enzyme exhibiting activity-dependent redox requirements. Sci Rep. 2017;7:7609.
34. Frago S, Martínez-Júlvez M, Serrano A, Medina M. Structural analysis of FAD synthetase from *Corynebacterium ammoniagenes*. BMC Microbiol. 2008;8:160.
35. Serrano A, Sebastián M, Arilla-Luna S, et al. The trimer interface in the quaternary structure of the bifunctional prokaryotic FAD synthetase from *Corynebacterium ammoniagenes*. Sci Rep. 2017;7:404.
36. Serrano A, Frago S, Herguedas B, Martinez-Julvez M, Velazquez-Campoy A, Medina M. Key residues at the riboflavin kinase catalytic site of the bifunctional riboflavin kinase/FMN adenylyltransferase from *Corynebacterium ammoniagenes*. Cell Biochem Biophys. 2013;65:57–68.
37. Sievers F, Wilm A, Dineen D, et al. Fast, scalable generation of high-quality protein multiple sequence alignments using Clustal Omega. Mol Syst Biol. 2011;7:539.
38. Capella-Gutiérrez S, Silla-Martínez JM, Gabaldón T. trimAl: A tool for automated alignment trimming in large-scale phylogenetic analyses. Bioinformatics. 2009;25:1972–1973.
39. Kumar S, Stecher G, Li M, Knyaz C, Tamura K. MEGA X: Molecular evolutionary genetics analysis across computing platforms. Mol Biol Evol. 2018;35:1547–1549.
40. Källberg M, Wang H, Wang S, et al. Template-based protein structure modeling using the RaptorX web server. Nat Protoc. 2012;7:1511–1522.
41. Ashkenazy H, Abadi S, Martz E, et al. ConSurf 2016: An improved methodology to estimate and visualize evolutionary conservation in macromolecules. Nucleic Acids Res. 2016;44:W344–W350.
42. Delano WL. PyMOL: An open-source molecular graphics tool. CCP4 Newsl Protein Crystallogr. 2002;40:82–92.
43. Jurrus E, Engel D, Star K, et al. Improvements to the APBS biomolecular solvation software suite. Protein Sci. 2018;27:112–128.
44. Serrano A, Arilla-Luna S, Medina M. Insights into the FMNAT active site of FAD synthase: Aromaticity is essential for flavin binding and catalysis. Int J Mol Sci. 2020;21:1–16.
45. Lee SS, McCormick DB. Effect of riboflavin status on hepatic activities of flavin-metabolizing enzymes in rats. J Nutr. 1983;113:2274–2279.
46. Torchetti EM, Bonomi F, Galluccio M, et al. Human FAD synthase (isoform 2): A component of the machinery that delivers FAD to apo-flavoproteins. FEBS J. 2011;278:4434–4449.
47. Lans I, Seco J, Serrano A, et al. The dimer-of-trimers assembly prevents catalysis at the transferase site of prokaryotic FAD synthase. Biophys J. 2018;115:988–995.
48. Serrano A, Sebastian M, Arilla-Luna S, et al. Quaternary organization in a bifunctional prokaryotic FAD synthetase: Involvement of an arginine at its adenylyltransferase module on the riboflavin kinase activity. Biochim Biophys Acta. 2015;1854:897–906.
49. Serrano A, Frago S, Velázquez-Campoy A, Medina M. Role of key residues at the flavin mononucleotide (FMN): Adenylyltransferase catalytic site of the bifunctional riboflavin kinase/flavin adenine dinucleotide (FAD) synthetase from *Corynebacterium ammoniagenes*. Int J Mol Sci. 2012;13:14492–14517.
50. Kearney EB, Goldenberg J, Lipsick J, Perl M. Flavokinase and FAD synthetase from *Bacillus subtilis* specific for reduced flavins. J Biol Chem. 1979;254:9551–9557.
51. Langer S, Hashimoto M, Hobl B, Mathes T, Mack M. Flavoproteins are potential targets for the antibiotic roseoflavin in *Escherichia coli*. J Bacteriol. 2013;195:4037–4045.
52. Torchetti EM, Brizio C, Colella M, et al. Mitochondrial localization of human FAD synthetase isoform 1. Mitochondrion. 2010;10:263–273.

SUPPORTING INFORMATION

Additional supporting information may be found in the online version of the article at the publisher's website.

How to cite this article: Moreno A, Taleb V, Sebastián M, Anoz-Carbonell E, Martínez-Júlvez M, Medina M. Cofactors and pathogens: Flavin mononucleotide and flavin adenine dinucleotide (FAD) biosynthesis by the FAD synthase from *Brucella ovis*. IUBMB Life. 2022;74:655–71. https://doi.org/10.1002/iub.2576